Check for updates

Continuous Flow Routes toward Designer Metal Nanocatalysts

*Joshua S. Santana and Sara E. Skrabalak**

Mono- and multimetallic nanoparticles (NPs) have diverse and tunable physicochemical properties that arise from their compositions as well as crystallite size and shape. The ability to control precisely the composition and structure of NPs through synthesis is central to achieving state-of-the-art designer metal NPs for use as catalysts and electrocatalysts. However, a major limitation to the use of designer metal NPs as catalysts is the ability to scale their syntheses while maintaining structural precision. To address this challenge, continuous flow routes to metal NPs involving the use of droplet microreactors are being developed, providing the synthetic versatility necessary to achieve known and completely new nanostructures. This progress report outlines how the chemistry and process parameters of droplet microreactors can be used to achieve high performing nanocatalysts through control of NP composition, size, shape, and architecture and outlines directions toward previously unimaginable nanostructures.

1. Introduction of Energy Challenges

Designing mono- and multimetallic nanoparticles (NPs) has been a hot topic over the last few decades as their applications include nanotherapy, chemical sensing, counterfeit detection, and more.[1] In fact, the study and use of metal NPs for catalysis and electrocatalysis are at an all-time high.[2] A catalyst accelerates a chemical reaction without being consumed and may aid in the selectivity of a reaction toward a certain pathway or product.[2] For example, nanocatalysts are used in proton exchange membrane fuel cells (PEMFCs) and batteries to help transport chemical energy to electricity through redox reactions at the anode and cathode of these devices.[3] However, even with catalysts, these processes often still have sluggish reaction kinetics, requiring further advances in the design of catalysts.[4] Traditionally, nanoscale catalysts have been prepared by methods that do not provide precise control over structure (e.g., incipient wetness impregnation).[5] However, nanocatalytsts with increased performance and limited catalyst poisoning and degradation can be achieved with designer NPs prepared by colloidal routes where particle size, shape, and architecture are precisely controlled, in addition to composition.[6]

Seemingly simple chemistry is often used to prepare metal NPs by colloidal methods, but the underlying nucleation and growth processes are complex, with new insight being gained every day.[7] These syntheses begin with the reduction or decomposition of a metal salt or complex, which occurs in the presence of molecules and/or ions that help to stabilize the growing particles in solution and direct growth.[8] These processes are very sensitive to the reaction conditions, wherein part per billion differences in reagent concentrations and small temperature fluctuations can alter growth pathways and limit product monodispersity.[9] This sensitivity also can limit large-scale production of nanomaterials as thermal equilibrium is difficult to maintain in large reaction vessels.[10] In order to produce designer metal nanocatalysts with structural and compositional precision on a large scale, new synthetic methods are required. Herein, this progress report discusses the underlying principles of designer metal nanocatalysts. Then, we examine the synthesis of such designer NPs in continuous-flow droplet reactors as such platforms can address the challenges associated with large-scale synthesis. We conclude by considering the flow synthesis of new nanocatalysts that may not be possible by batch methods.

2. Design Criteria of Nanocatalysts

In order to achieve high performing designer metal nanocatalysts, composition, particle size and shape, and overall architecture all must be considered as each can influence what surface–adsorbate interactions are possible and the strength of these interactions.

2.1. Composition

Both mono- and multimetallic compositions can make for high performing nanocatalysts, where the metal(s) chosen define the nature of surface–adsorbate interactions. In accordance with the Sabatier principle, high reactions rates are achieved with catalysts when reaction intermediates do not bind too weakly or too strongly to the catalytic surface.[11] This binding energy is consistent with the d-band model of catalysis proposed by

---

J. S. Santana, Prof. S. E. Skrabalak
Department of Chemistry
Indiana University–Bloomington
800 E. Kirkwood Ave., Bloomington, IN 47405, USA
E-mail: sskrabal@indiana.edu

The ORCID identification number(s) for the author(s) of this article can be found under https://doi.org/10.1002/aenm.201902051.

DOI: 10.1002/aenm.201902051

Hammer and Nørskov, which states that the molecular adsorption energy is primarily dependent on the occupancy of the bonding and antibonding states formed by the hybridization of the wave functions between the adsorbates and the d-state electrons of the metal.[12] Thus, when the antibonding state is below the Fermi level (E_F), the adsorbate and metal surface become repulsive, causing weak adsorption. In contrast, strong binding occurs when the antibonding state is above the E_F.[13] Therefore, the position of the d-band center (ε_d) characterizes the strength of the binding and can be tuned to achieve maximum rates.

When considering alloys, mixing precious metals with earth-abundant elements can yield cost effective materials. Moreover, the nature of the surface–adsorbate interaction depends on the atomic arrangement of the different metal types, modifying the electronic structure of the surface through ligand effects and the types of sites available through geometric (ensemble) effects. Ligand effects refer to electron donation from one atomic center to another through differences in work function. Atoms with lower work functions will donate electrons to atoms with higher work functions, increasing the number of filled orbitals.[4] This charge donation will lower the ε_d, to weaken surface–adsorbate interactions.[14] Markovic and co-workers showed the impact of alloying by mixing Pt with different 3d transition metals, creating a catalogue of bimetallic Pt-containing surfaces. The specific activities of the NP products toward the oxygen reduction reaction (ORR) were measured and correlated with their ε_d.[15]

Geometric (ensemble) effects refer to the atomic arrangement at the catalyst surface which is available for adsorbate binding and can dictate molecular orientation and, in turn, catalytic pathways.[16] With monometallic NPs, which facets are expressed govern molecular orientation. However, incorporation of more than one metal in the form of an alloy will provide different types of sites that depend on the ratio of metals in the alloy (e.g., clustering or single site isolation).[16a] For example, clustering of active sites may cause adsorbates to bind in a bridge or hollow site.

A special class of multimetallic NPs being evaluated as catalysts is those with atomic ordering, i.e., intermetallic phases. In contrast to random alloys where the different atom types are arranged in statistically random positions throughout the lattice, intermetallics exhibit long-range chemical ordering, with each crystallographic site occupying a fixed atomic site.[17] **Figure 1** (middle ring, bottom section) provides an example of an intermetallic lattice compared to a random alloy lattice.[18] The interest in intermetallic phases stems from their ordered crystal structures providing atomically precise multimetallic surfaces for catalysis. Moreover, their lower heats of formation can provide more robust catalysts, especially for electrocatalytic processes where the highly corrosive environments can lead to metal leaching. In addition, intermetallics have shown different catalytic activities than their random alloy counterparts.[19] In fact, Wang and co-workers showed that intermetallic PdCu NPs have higher specific and mass activities toward the ORR compared to random alloy PdCu NPs as well as greater durability.[20]

2.2. Size

NP size is an important criterion in designing nanocatalysts as it can directly impact utility. Typically, NPs in the 1–10 nm size range are preferred for applications in catalysis.[21] This preference is because the surface-to-volume ratio is enhanced in this size regime, making the materials more cost-effective.[22] When manipulating the size of NPs, faceting and electronic structure also can change. For example, Pt NPs with diameters ranging from 1 to 5 nm were used as catalysts for the ORR,[23] with the specific activity being greatly diminished as the diameter of the NPs fell under 2.5 nm. This decrease was attributed to oxygen binding too tightly at edge and vertex sites on the Pt NPs, which increase in concentration with shorter particle diameter.

In addition to binding strength hindering activity, NP size can influence the selectivity of a desired product.[24] This dependence was demonstrated with carbon-supported Pt NPs used as a catalyst for the carbon–nitrogen ring opening reaction of pyrrole. Pt NPs from 0.8–5 nm were evaluated and each size had a different selectivity toward different pyrrole derivatives. The larger Pt NPs produced almost entirely *n*-butylamine, whereas the smaller NPs formed a combination of pyrrolidine and *n*-butylamine.[25] Because of the differing electronic structure and faceting with NP size, choosing NPs of appropriate size is critical to achieving high performance catalysts.[22]

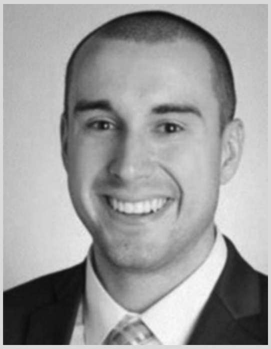

Joshua S. Santana received his B.A. degree in chemistry from Wabash College in Crawfordsville, IN, in 2015 where he conducted research with Professor Laura Wysocki. He then moved to the Indiana University where he has been working on his Ph.D. in materials chemistry under the tutelage of Professor Sara E. Skrabalak. His interests focus on the advancement of nanotechnology, specifically regarding sustainable energy.

Sara E. Skrabalak received her B.A. degree (chemistry) from Washington University in St. Louis in 2002, conducting research with Professor William Buhro. She then moved to the University of Illinois at Urbana–Champaign where she completed her Ph.D. degree (chemistry) in 2006 under the tutelage of Professor Kenneth Suslick. After conducting postdoctoral research at the University of Washington–Seattle with Professors Younan Xia and Xingde Li, she began working at Indiana University–Bloomington where she is the James H. Rudy Professor. Her group develops new methods to structurally defined materials and studies their properties for applications in energy science, chemical sensing, and secured electronics.

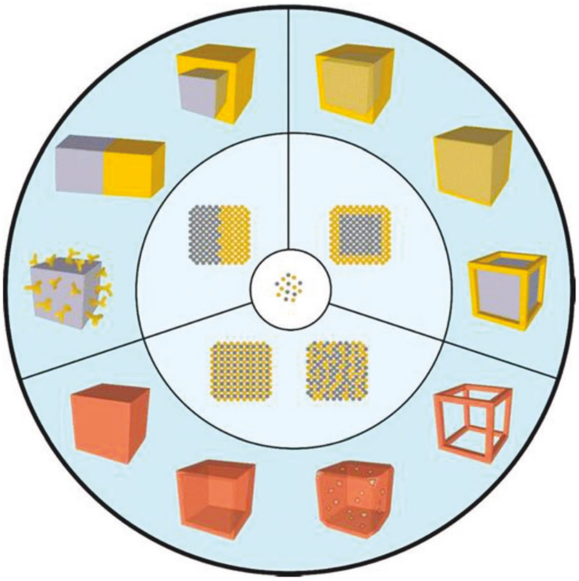

Figure 1. Scheme showing different NP architectures that evolve from two types of metal atoms (center). Middle ring: Four types of atomic distributions possible with two metal atom types. Outer ring: Examples of many bimetallic nanocrystals with distinct architectures. The two different atoms have a yellow and gray color, while an alloy or intermetallic compound has an orange color. Adapted with permission.[18] Copyright 2016, American Chemical Society.

2.3. Shape

Beyond NP size, the shape of a particle will directly affect the catalytic performance as different facets are exposed.[26] Specifically, adsorption energetics and diffusion/reaction pathways change with different facets.[27] For example, Pt icosahedra containing {111} facets were found to have a specific activity toward the ORR ≈3 times greater than Pt nanocubes containing {100} facets.[28] This difference was attributed to the adsorption of OH_{ads} being more favorable to low-index Pt surfaces and the twinning-assisted, strained surface lattice of icosahedral nanocrystals. Furthermore, this shape effect holds for multimetallic systems. For example, core@shell Au@Pd concave cubes outperformed core@shell Au@Pd octahedra in catalyzing Suzuki coupling of iodobenzene and phenylbroronic acid because the concave cubes expose desirable high-index facets.[6c]

NPs of different shapes are accessed by manipulating nucleation and growth conditions.[26a] Products can vary between low energy structures, e.g., a Wulff polyhedra of an fcc metal, to higher energy kinetic products, e.g., branched NPs with high index facets.[29] Thermodynamic products are lower in total free energy but require a higher activation energy compared to the kinetic products, thus a larger thermal energy input is needed to access thermodynamic structures. Thermodynamic versus kinetic control has been demonstrated in a variety of systems, where the product is dependent on the thermal energy input and solvent conditions.[29,30] As NP shape defines the surfaces that are expressed, the development of syntheses to shape-controlled NPs is critical to achieving high performance catalysts.

2.4. Architecture

Finally, NP architecture can be important to catalytic performance and refers to how different material domains are distributed in 3D space. Examples of different metal NP architectures are hollow/porous structures for increased surface area, dimers and heterostructures for spillover effects in catalysis, and core@shell structures for strain effects.[18] These architectures are highlighted in the outer ring of Figure 1.[18] This figure corresponds to bimetallic systems, but one can derive from this scheme how different architectures also apply to mono- and higher multimetallic systems. Hollow/porous structures tend to be more catalytically active by mass due to access of interior and exterior walls.[31] Dimers and other heterostructures can put metals with different properties adjacent to one another, enabling one reaction step to occur at one metal domain and then proceed at a nearby, but different, metal domain.[18]

Core@shell particles are often desirable for their strain (tensile versus compressive) effects that can tune the ε_d. Both tensile and compressive strain can be engineered into core@shell NPs depending on their composition and architecture, as can be seen in **Figure 2**.[4] For tensile strain, the depositing shell lattice is smaller than the surface; this condition causes decreased orbital overlap and raises the ε_d. Compressive strain is achieved when a material with a larger lattice is deposited as a shell; this condition causes increased orbital overlap and lowers the ε_d.[32] By manipulating the strain on the surface of the particle, adsorption strengths can be tailored with the goal of following the Sabatier principle to achieve maximized reaction rates.

Seed-mediated growth is typically used to achieve bimetallic NPs with different architectures, and consideration of the atomic radii, bond dissociation energies, and electronegativities of the seed metal relative to the depositing metal are important to achieving core@shell structures as opposed to other architectures. For epitaxial layered growth of one metal on a seed of another metal, i) the lattice constants of the two metals should be comparable, with the lattice mismatch smaller than about 5%; ii) the electronegativity of the shell metal should be lower

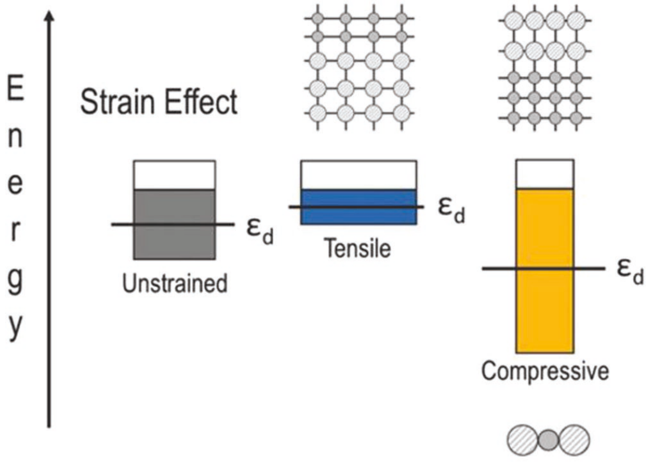

Figure 2. Scheme of how the strain effects tailor the d-band center for bimetallic NPs. Adapted with permission.[4] Copyright 2018, Wiley-VCH.

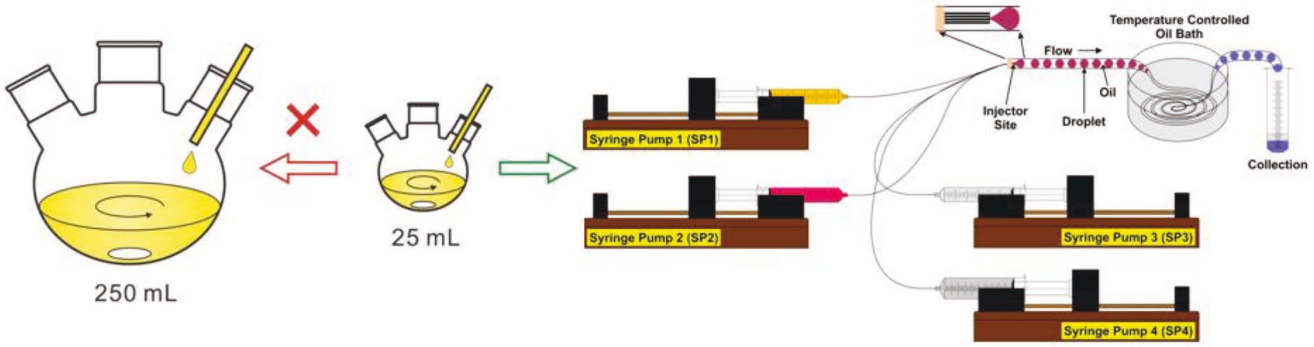

Figure 3. A comparison of two opposite synthetic methods for the scaling up of metal NP products. These two methods include increasing the reaction solution (left, batch reaction)[36] or decreasing the reaction solution (right, microreactor).[39] Adapted with permission.[36,39] Copyright 2014, Wiley-VCH and Copyright 2017, American Chemical Society.

than the core metal in order to avoid the displacement reaction and to easily wet the surface of the core; iii) the bond energy between the metal atoms of the shell should be smaller than that between the shell atoms and substrate atoms in order to ensure the Frank–van der Merwe layer-by-layer growth.[33] If these factors are not met, Volmer–Weber growth or Stanski–Krastanow growth could dominate, eliminating conformal epitaxial growth and giving rise to different overall shapes and architectures of the NPs.[34] These type of predictive guidelines are important considerations when designing NPs for catalytic applications.

3. Traditional Synthetic Methods

Methods like incipient wetness impregnation have been used commonly to make industrial metal catalysts.[5] While successful in producing useful materials, these methods yield ill-defined materials, which results in great efforts being directed toward understanding the origin of performance and active site identification. In contrast, designer nanocatalysts are usually inspired by surface science studies and computational tools and aim to express optimized active sites through precise control of composition and structure. Designer metal NPs are traditionally synthesized by colloidal methods in batch reactions because of the facile reaction setup, ability to fine-tune reaction parameters, and proven capabilities to synthesize monodisperse products.[35] However, these methods typically produce only mg quantities of NPs, limiting their use in applications where much more material is required. One major limitation to larger scale production is the difficulty to maintain thermal equilibrium (the ability to maintain constant temperature) throughout a large reaction vessel.[36] Subtle changes in reaction temperature can cause a range of nanoproducts.[9] In multimetallic NP synthesis, maintaining thermal equilibrium is even more important as a vast range of kinetic products are achievable at lower activation energies.[29] Without thermal equilibrium, these multimetallic NPs can range from branched NPs to conformal NPs, with a variety of sizes, shapes, and architectures in between.[29] Because of the issues with scaling traditional synthetic techniques for metal NPs, new methodologies are being explored to produce designer NPs for diverse applications, including for catalysis where composition, particle size and shape, and overall architecture must be precisely controlled.

4. Continuous Droplet Reactors

A recent and promising synthetic method for the scale-up of metal NPs is continuous-flow droplet reactors due to the continuous production of small reaction droplets (**Figure 3**).[36,37] These continuous-flow droplet reactors can confine reactions in the microliter regime, giving rise to the term microreactor, allowing thermal equilibrium and mass transport (i.e., convection, diffusion, and migration) to be better controlled compared to large-scale batch reactions.[10,38] In fact, microreactors have been used to synthesized metal NPs not yet achieved in batch reactions.[37e] Additionally, continuous microreactors have environmental health and safety benefits, making them practical platforms for industrial automation and commercialization.[37f] An example of a continuous-flow droplet microreactor can be seen on the right side of Figure 3.[39] Generally, these two-phase microreactors have reagent-filled syringes placed on syringe pumps, with one syringe containing an immiscible carrier fluid.[40] These syringes are connected to the carrier tubing often through silica capillaries, as silica capillaries are inert to common metal NP reagents, but other construction materials may be considered. As the syringe pumps push reagent material into the carrier tubing, reaction droplets are created through the two immiscible phases, which are simultaneously injected into the flow tubing at an optimal ratio.[41] These reaction droplets can be heated inline for a desired residence time before exiting the tubing into a collection vessel. This fundamental microreactor setup can be differentiated depending on the system.[42] These types of microreactors have been applicable to many different chemistries, including automated synchronization of bacterial cells, organic polymer production, small organic molecule synthesis, quantum dots formation, and more.[43] However, this discussion will focus on microreactor techniques that are capable of synthesizing known and new metal NP structures. We especially focus on strategies to achieve favorable designer nanostructures for catalysis. Herein, the different synthetic parameters applicable to continuous-flow droplet microreactors are dissected for metal NP syntheses.

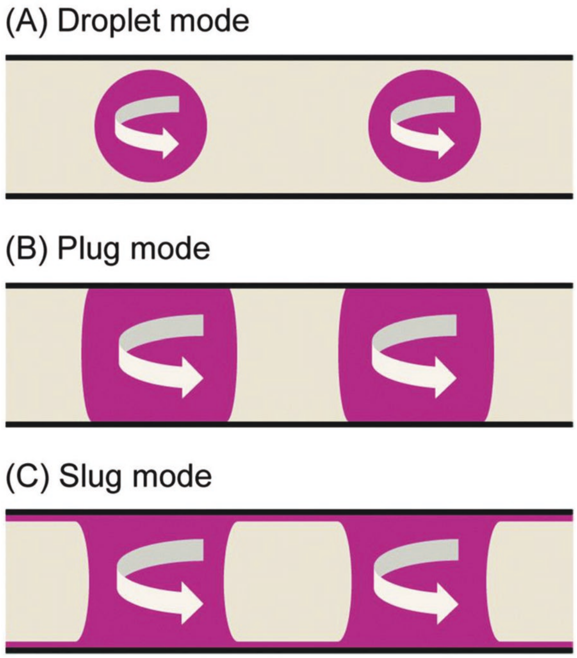

Figure 4. Representations of three flow modes in continuous-droplet reactors. A) Droplet mode, where the droplet is isolated from the channel wall. B) Plug mode, where the convex droplet contacts both the wall and carrier fluid. C) Slug mode, where the concave droplet contacts both the wall and carrier fluid. Adapted with permission.[10] Copyright 2015, Royal Society of Chemistry.

5. Reaction Parameters for Continuous-Flow Droplet Microreactors

5.1. Flow Modes

Flow modes in microreactors can adopt either droplet, plug, or slug mode as depicted in **Figure 4**.[10] In droplet mode, the reaction droplet is completely encompassed by an immiscible carrier fluid, creating only one interface for the reaction droplets. Interestingly, surfactants with hydrophobic tails are often used in metal NP synthesis to provide colloidal stability and direct particle shape; these surfactants can interact at the droplet interface (interfacial adsorption), causing polydispersion.[44] To alleviate this effect in microreactor syntheses of NPs, nonionic surfactants are being used.[44] For example, in a seeded-growth synthesis of Ag nanocubes (where poly(vinylpyrrolidinone) (PVP) was the capping agent and L-ascorbic acid (L-aa) was the reducing agent) in a two-phase microreactor, interfacial adsorption was alleviated with Triton X-100, a nonionic surfactant, which produced more monodisperse Ag nanocubes compared to the synthesis when Triton X-100 was absent.[44] The absence of Triton X-100 resulted in self-nucleation of Ag, forming small particles and some large irregular-shaped particles. Furthermore, the researchers claimed Triton X-100 did not affect the capping effects of the PVP since most seeds adsorbed onto the water-oil interface in reactions without Triton X-100, leaving behind fewer seeds in the aqueous phase for growth.

In plug mode, the reaction interface is more complex as there are now two interfaces. One interface is the reaction phase with the immiscible carrier fluid, as in droplet mode, and the other is from contact between the reaction phase and the carrier tubing. As the entire reaction plug is not surrounded by the immiscible phase, interfacial adsorption is not homogenous and the two interfaces may have subtle, but different, convection dynamics. This mode is common because popular immiscible and reaction phases (i.e., silicone oil and water) generally yield plug mode dynamics, but the inhomogeneity and the differing convection dynamics must be considered for sensitive metal NP growth modes.

Lastly, slug mode contains a reaction phase that is in contact with the reaction tubing and neighboring slugs. Reaction solvents used for this mode need to have a strong affinity for the inner wall of the reaction tubing, resulting in a concave shape for the reaction slug. However, the slug mode should be avoided as contact between reaction slugs allows for diffusion throughout the microreactor.

5.2. Mixing

Inducing mixing in microreactor reactions is not as straight forward as controlling the stirring in batch reactions. However, ensuring well-mixed reagents in droplets is central to achieving high quality products. There are a variety of techniques employed depending on the microreactor system and the number of lines being introduced to create the droplets. It is worth noting that in many cases, different reagents are held in different syringes to inhibit reaction or side processes until droplets are well mixed and delivered to a heating zone. One technique to achieve mixing is to increase the overall flow rate, where the flow can be categorized as laminar, vortex, or turbulent jet.[45] Typically, laminar flow dominates at slow flow rates, causing slower mixing. As the flow rate increases, vortex and then turbulent jet flow becomes prominent, inducing faster mixing.[46]

Three other mixing methodologies can be seen in **Figure 5** and include chaotic advection, pinched zones, and electrocoalescence.[10] As shown in Figure 5A, chaotic advection aids in mixing within droplets by rapidly reorienting the direction of the droplet as it follows a bent path. As this droplet changes from bent pathways to straight pathways, internal recirculating flow folds and stretches the droplet, increasing reagent mixing.[10] This rapid strategy is a simple and effective way to achieve adequate mixing in confined reactions.[47] Mixing can also be achieved by pinching the reaction tubing at precise intervals as shown in Figure 5B for the synthesis of Au NPs. Transmission electron microscopy (TEM) images of Au NPs synthesized without and with pinched zones are shown in Figure 5B where monodispersity is increased with pinching due to increased mixing within the reaction. However, droplets can fuse together if the pinched zones occur too close to one another.[41] Finally, mixing within microreactor droplets can be achieved through electrocoalescence (Figure 5C).[48] In this process, two adjacent droplets are exposed to a high electric field in order to combine the droplets.[49] This process has been used for reagent addition in metal NP microreactor reactions, but could cause alternative growth pathways through manipulating growth kinetics to produce dendritic structures.[50] These growth effects will be discussed further in Section 5.8, where

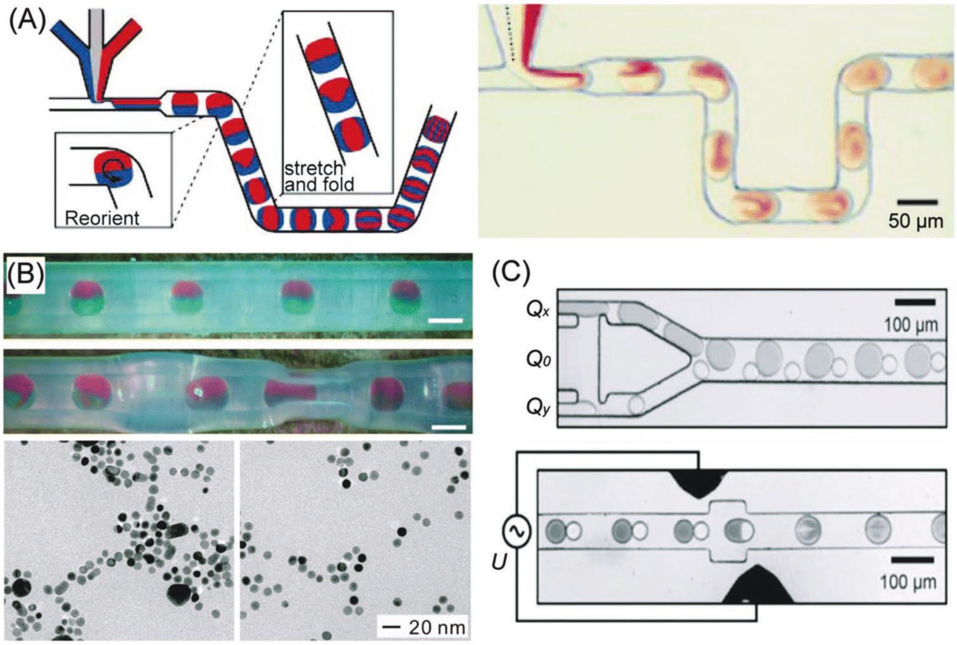

Figure 5. Representation of three ways to achieve mixing in droplet reactors. A) Use of winding zones in the reaction line to achieve chaotic advection in droplets. The left panel shows a schematic representation and the right panel is an optical image of chaotic advection in winding zones. B) Use of pinched zones to induces droplet mixing. The top panel shows an optical image of nonpinched zones versus pinched zones. The bottom images are TEM images of Au NPs with the left particles being synthesized without pinched zones and the right particles synthesized with pinched zones. C) Use of electrocoalescence to induce droplet mixing. The top image is a without an electric field and the bottom includes an electric field. Adapted with permission.[10] Copyright 2015, Royal Society of Chemistry.

multistep reactor processes are discussed. The versatility of these mixing processes allows for a catalogue of microreactor reaction enhancements when developing a system.

5.3. Reaction Volume

The reaction volume of the droplet can be manipulated to achieve different reaction conditions. The reaction-droplet length can be determined by the ratio

$$L/W = \frac{1 + \alpha Q_{\text{reaction}}}{Q_{\text{immiscible}}} \tag{1}$$

where L is the length of the droplet containing the reaction, W is the width of the tubing channel, Q is the flow rates of the reaction and immiscible phases, and α is a constant related to the junction where the formation of the reaction droplet occurs.[10,41] Typically, these reaction droplets are in the micro- to milliliter regime to ensure thermal equilibrium during metal NP synthesis.[51] The use of larger droplets leads to faster production of the metal NPs; however, thermal equilibrium can be difficult to maintain (just as in batch reactions). Thermal equilibrium is better maintained with smaller droplets; however, the rate of product production will be slower. This dependence leads to a balancing act wherein reaction droplets should be large enough to produce as much product as possible, but small enough to ensure thermal equilibrium is achieved to create a monodisperse product.

Alternatively, parallel microfluidic-droplet reactors are a viable route to large-scale production of colloidal inorganic NPs.[52] However, a major challenge in designing and implementing parallel microreactor systems is guaranteeing uniform fluidic behavior throughout the ensemble.[53] Brutchey and co-workers reported a 3D droplet microreactor with four-branched parallel networks capable of producing statistically indifferent Pt NPs.[54] This parallel network was shown to be insensitive to small changes that could arise due to feedback between channels. This parallel methodology doubled the reaction productivity of the Pt NPs compared to the analogous batch synthesis. Through manipulating the droplet volume and designing parallel microreactor systems, the scale-up of NP product is viable.

5.4. Heating Element

Many metal NP syntheses require heating to facilitate the nucleation and growth process, and the thermal input allows the structural features of the NPs to be tuned as mentioned toward either kinetic or thermodynamic products. Typically, the microreactor tubing is fed through a temperature-controlled oil bath, although other thermal inputs can be used; the tubing length and droplet flow rate determine the residence time for a reaction.[41] Thus, in addition to the temperature of the oil bath impacting the compositional and structural features of the NPs, the residence time can influence these features. For example, online measurements through UV–vis spectroscopy integrated into a microreactor, where chloroauric acid ($HAuCl_4$) was reduced by L-aa in the presence of PVP, showed that the mean diameters for Au NPs were dependent on the residence time of the reaction.[55] Therefore, residence time needs to be considered to optimize surface-to-volume ratios of nanocatalysts, while maintaining the desired shape.

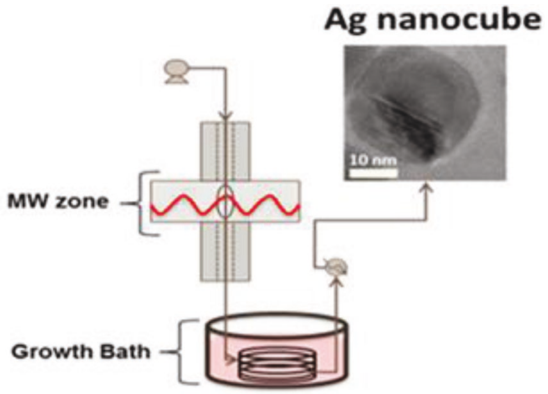

Figure 6. A microreactor scheme showing the use of a microwave heating zone and a growth bath heating zone to separate nucleation and growth processes during Ag nanocube reactions, respectively. This figure also includes a transmission electron microscopy image of the Ag nanocubes synthesized in the microreactor. Adapted with permission.[58] Copyright 2017, American Chemical Society.

Recently, microwave-mediated radio frequency (RF) heating, instead of thermal addition through an oil bath, has been used to facilitate the chemistry for metal NP formation.[56] Specifically, Rh NPs were synthesized ranging from cubo-octahedra to branched multipods using a microwave heating unit through manipulating the phase (single-phase or two-phase), temperature, and/or residence time.[56] The range of Rh NPs synthesized exhibit different sizes and facets that could lead to differences in catalytic performance. The Rh multipods were made possible as the microwave heating element can cause specific product growth via dipolar coupling of microwaves with polar charged species.[56] In addition, RF heating has been hypothesized to create hot spots on metal NPs, impacting the synthetic outcome.[57]

There has been an effort to separate nucleation events from growth events during NP synthesis by sequentially utilizing an RF heating unit and a temperature-controlled oil bath unit.[58] **Figure 6** shows a scheme of this multistep reactor using both heating components as well as a TEM image of the Ag nanocubes synthesized in the microreactor.[58] Initially, the reagents flowed through the microwave zone to synthesize spherical Ag NPs. Next, the spherical NPs flowed through a growth bath where the particles became more cubic with increased residence time. This strategy has the potential to provide distinct kinetic regimes for NP formation and access to unique NP shapes and architectures.

5.5. Initial Concentrations

Another control parameter of droplet microreactors for metal NP synthesis is the ability to tailor the initial concentrations in the starting reagent syringes. The dependence of metal NP product on initial concentrations arises because the reagent concentrations directly correlate with supersaturation. NPs nucleate and grow when a solution becomes supersaturated. Therefore, NPs of different sizes and shapes can be achieved through manipulating supersaturation conditions.[41] For example, tailoring the size and morphology of Pd NPs has been demonstrated in microreactor reactions by manipulating the reducing agent and capping agent concentrations in the starting syringes, while keeping flow rates constant.[41] Specifically, with increasing reducing agent (L-aa) concentration in the starting syringe, Pd NPs produced from the reduction of Na_2PdCl_4 in the presence of PVP and potassium bromide (KBr) went from spherically shaped to sharp cubes.

Considering the synthesis of bimetallic NPs with architectural control, Pt branches have been deposited on Pd nanocubes using a microreactor where the branch length could be precisely controlled through reagent concentrations.[59] Specifically, Pt branches were grown on cubic Pd seeds by reducing K_2PtCl_4 in the presence of L-aa, KBr, and PVP. Increasing the concentrations of the K_2PtCl_4 and L-aa in their starting syringes, while keeping flow rates constant, produced longer branches off the vertices of the Pd cubes. This synthesis demonstrates NP compositional control by manipulating the ratio of Pd:Pt in the final structure. In addition, architectural control is achieved by tailoring the size of the Pt domains off the vertices of the Pd cube. Similar Pd–Pt particles have been prepared in batch reactions and have been shown to be excellent catalysts for the ORR, formic acid oxidation, and methanol oxidation.[60]

5.6. Flow Rates

As mentioned in Section 5.2, the flow rate determines whether the flow is a laminar, vortex, or turbulent jet.[45] These different regimes affect the mixing and interface between the two mediums. In addition to varying the overall flow rate, manipulating the relative flow rates of the microreactor reagent solutions inline (on-the-fly) can change the metal NP product. This concept was demonstrated with the synthesis of core@shell Au@Pd nanostructures where different conformal Pd shell thicknesses were deposited on cubic Au seeds in the presence of cetyltrimethylammonium chloride (CTAC), sodium bromide (NaBr), and L-aa.[39] By changing the relative flow rates of the metal Pd precursor with respect to the Au cubic seeds, while keeping the total additive flow rate constant, conformal Pd shell thicknesses deposited on the cubic Au seeds were controlled. **Figure 7** shows the range of Au@Pd core@shell nanostructures synthesized using this flow rate manipulation process. As the flow rate of the cubic Au seed solution was decreased and the flow rate of the Pd precursor reagent solution was increased, while keeping the total additive flow rate constant, Pd shell thicknesses on the exterior of the Au seeds were increased. At high Pd precursor flow rate relative to cubic Au seeds, homogenous Pd appeared due the high supersaturation the Pd precursor. This process was effective in depositing a range of Pd dendritic shells on Au octahedral seeds, as well.[39] This methodology shows architectural control of NPs inline instead of having to change stock solutions, which limits synthetic waste. Depositing conformal Pd shells on Au seeds puts the Pd shell under tensile strain. In tensile strain, the depositing lattice is smaller than the surface causing decreased orbital overlap, thus raising the ε_d. However, the ε_d can be manipulated through varying the shell thickness of the NP allowing this inline synthetic-control method to be a great way to synthesize nanocatalysts. In fact, similar core@shell Au@Pd structures prepared in batch reactions have been shown to be excellent catalysts for Suzuki coupling reactions, methanol oxidation, and formic acid electrooxidation.[6c,61]

Recently, this methodology was extended to kinetically controlling the shape of NPs inline by manipulating relative flow

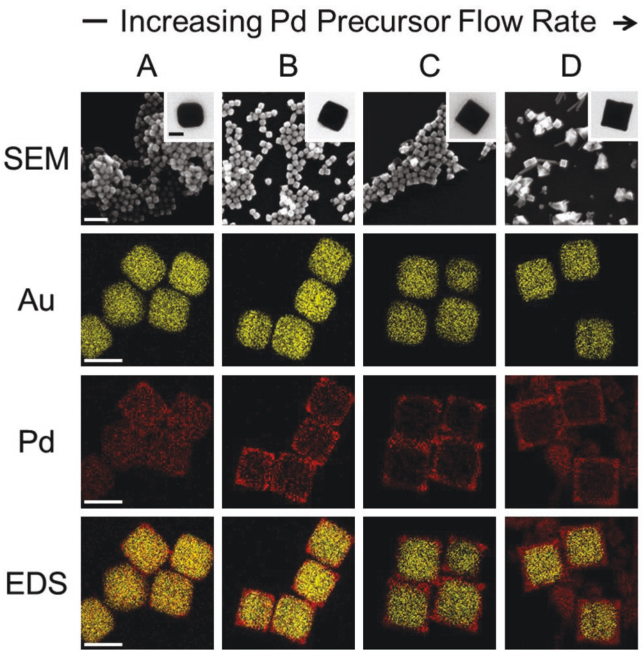

Figure 7. Example of dimensional control with Au@Pd NPs achieved in a continuous-droplet microreactor through manipulating relative flow rates, not stock solutions. This was achieved through increasing the Pd precursor flow rate while decreasing the Au seed flow rate. Row SEM: Images of the Au@Pd particles (inset: TEM; scale bars: 25 nm) with scale bars 200 nm. Rows Au, Pd, and EDS: Elemental mapping of Au signal, Pd signal, and the overlay of the Au and Pd signals (yellow = Au; red = Pd). Scale bars are 50 nm. Adapted with permission.[39] Copyright 2017, American Chemical Society.

rates.[62] In this study, the inline manipulation of reagent flow rates allowed a range of products from kinetically favored Au–Pd sharp-branched octopods to thermodynamically favored core@shell octahedra to be successfully synthesized. These structures were achieved by manipulating the pH in solution through flow rate manipulations, thus changing the reducing capability of the L-aa solution. At high pH, the rate of deposition was favored as adatoms were kinetically trapped at high energy site generating branched octopod structures, thus kinetic control. As the pH was lowered, the reducing capability of the L-aa was weakened, allowing the rate of diffusion to dominate. When the rate of diffusion dominated, the adatoms could diffuse to more favorable sites, generating core@shell octahedra. Accessing these different NP shapes that express different facets give rise to a catalogue of synthesized nanocatalysts where the catalytic performance is based on the exposed facets. It is expected that the high-index facets exposed on the octopods will exhibit different catalytic performance than the (111) faceted octahedra.

5.7. Hydrophobicity

The material selected to hold the flowing droplets can also influence the product as droplet formation and fluidic dynamics change with interfacial energies. Typically, hydrophobic tubing (polytetrafluoroethylene, PTFE) encompasses aqueous droplet reactions separated by organic media, where the organic media can be tuned to vary interfacial thicknesses.[63] Additionally, the hydrophobicity of the tubing plays a role by affecting the curvature of the fluids, which correlates with reagent diffusion within the media.[64] To evaluate how different hydrophobic reaction lines in microreactors lead to different diffusion mechanisms and NP products, an aqueous/organic two-phase systems was flowed through either a hydrophobic PTFE microreactor or a hydrophilic Si–Pyrex microreactor.[65] In this two phase system, Au NPs were synthesized by adding $HAuCl_4$ and CTAB to the aqueous phase and using toluene as the organic phase. Because toluene served as the reducing agent for the Au precursor, reduction and growth occurred at the aqueous/organic interface. By manipulating the hydrophobicity of the microreactor, the aqueous/organic interface was modified causing different diffusion mechanisms in the system. When the microreactor had a hydrophobic wall (PTFE tubing), the aqueous reactions were confined in a plug mode. This is represented in **Figure 8**a,b. As the media flows through the

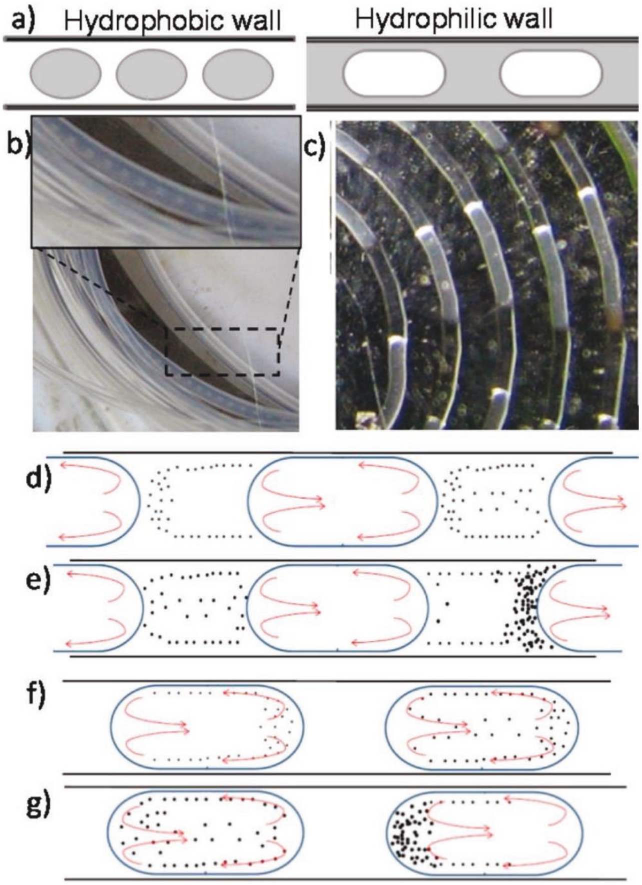

Figure 8. Scheme of the flow in microchannels with different hydrophobicities. a) Scheme of the differences in a hydrophobic versus hydrophilic wall where the aqueous phase is shown in gray while the organic phase is shown in white. b,c) Optical images of the hydrophobic versus hydrophilic microchannel reactions. d,e) Nanostructure formation sequence in hydrophilic Si microchannel reactor. f,g) Nanostructure formation sequence in a hydrophobic PTFE tube. Schematics in panels (d)–(g) are along the length of the microchannel at discrete locations from inlet (left) to the outlet (right). The flow of liquids is from inlet to the outlet (left to right). Adapted with permission.[65] Copyright 2017, American Chemical Society.

reaction tubing, the nanostructure formation accumulates at the back of the aqueous droplet where the fluid dynamics allow the aqueous reagents to interact with the organic reagents as seen in Figure 8f,g. This reaction method produced 12 nm NPs with shapes ranging from spheres to hexagonal plates. However, when the microreactor had hydrophilic walls (Si–Pyrex microreactor), the reactions took the form of the slug mode, which is shown in Figure 8a,c. As the media flows through the reaction tubing in this system, the nanostructure formation accumulates at the front of the aqueous phase where the fluid dynamics allow the aqueous reagents to interact with the organic reagents as seen in Figure 8d,e. This reaction method produced monodisperse hexagonal plates with an average diagonal distance around 42 nm. The reason different NPs were synthetized with different hydrophobic reaction lines is due to the availably of reagent materials at the interface as reagent material diffuses within the system. To produce monodisperse NPs in microreactors, diffusion mechanisms must be carefully understood as these mechanisms can lead to product differences and inhomogeneity issues.

5.8. Reactors Capable of Multistep Processes

Microreactors have been typically limited to one synthesis inline, which could limit the continuous-flow production of many shape and architecturally controlled NPs as they are traditionally produced by sequential batch processes wherein NP seeds are produced first. However, multistep microreactors for NP synthesis are appearing like the microwave and oil bath example that separates nucleation and growth processes.[58] Furthermore, these microreactors can be broken down into two complete growth segments for an initial seed growth followed by overgrowth of a secondary metal. Recent studies have used electrocoalescence (the mixing process briefly mentioned in Section 5.2) in a multistep microreactor to deposit Pd metal onto Au cores by first synthesizing Au spherical seeds followed by overgrowth of Pd metal in one continuous flow.[50] After the Au seeds were successfully synthesized in aqueous droplet reactions, aqueous miniemulsions containing overgrowth reagents were added to the Au reaction droplets by exposing the reaction tubing to a high electric field in order to combine the droplets and miniemulsions.[50] Adding an external field can cause alternative growth patterns and may be the reason for the dendritic-like Pd shells. However, these dendritic shells expose undercoordinated surface sites and a high surface-to-volume ratio, allowing these NPs to serve as excellent catalysts.

Other multistep reactors have appeared in the literature without reagent addition through electrocoalescence. These types of microreactor setups prevent external effects from electrocoalescence during growth processes and allow deposition to be based on reagent and reaction conditions. In fact, a multistep microreactor was used to synthesize the structurally controlled Pd–Pt heterostructures described in Section 5.5 where Pt branches grew from cubic Pd seeds.[59] Specifically, stage one of the multistep microreactor was used to synthesize cubic Pd NPs by reducing Na_2PdCl_4 with L-aa in the presence of PVP and KBr. These NPs were then used as seeds for Pt overgrowth downstream, where K_2PtCl_4 was reduced by L-aa in the presence of the Pd cubes, PVP, and KBr. Again, the length of the Pt branches was controlled by the initial reagent concentrations. The advancement of these multistep microreactors opens new pathways for different nanomaterial architectures to be synthesized inline, rather than having to use different reaction setups for seed and overgrowth syntheses.

6. Case Studies

6.1. Monometallic Systems

Monometallic NPs synthesized in batches have been evaluated and used as catalysts for the past few decades. Moreover, Ni NPs have been made using this batch methodology for catalyzing organic reactions, including the hydrolysis of the ammonia–borane (H_3NBH_3) complex.[66] Brutchey and co-workers advanced Ni NP syntheses by developing a high-throughput continuous flow synthesis to produce Ni NPs.[67] Their synthetic reactor is **Figure 9**A, which is modified from conventional continuous-flow microreactors. Their fluidic reactor uses a constant precursor flow rate that is monitored through a feedback loop between an analytical balance and pressurized gas. The balance allows the precursor solution of $Ni(acac)_2$, oleylamine, octadecene, and trioctylposphine to be monitored in real time, thus adjusting the pressure to maintain the constant flow rate. Following the balance portion of the reactor, the precursors flowed into a 220 °C conventional oven, resulting in fast nucleation and leading to small Ni NPs around ≈11 nm, which can be seen in Figure 9B. This synthetic method achieved yields of >60%, which was better than analogous batch reactions that gave only a 45% yield. The Ni NPs synthesized in flow and the Ni NPs synthesized in batch reactions were supported on SiO_2 and evaluated as catalysts for the deoxygenation of guaiacol (Figure 9C). The Ni NPs synthesized in the flow reactor and in batch greatly outperformed Ni/SiO_2 catalysts prepared through traditional incipient wetness techniques. The enhanced performance of the Ni NPs synthesized in the flow reactor and in batch arises because of their enhanced morphological control and narrow size distributions. Furthermore, the Ni NPs synthesized in the flow reactor and in batch exhibited similar H-adsorption site densities, site-time yields, and selectivities toward deoxygenated products. However, the flow reactor allows >27 g per day of the Ni NP product to be made, which is a more effective scale-up method than the analogous batch reactions.

Monometallic Au NPs have also been used as catalytic material traditionally made in batch reactions. This dates back to 1973 where Au NPs were synthesized and evaluated as a useful catalyst for olefin hydrogenation.[68] In 2017, Grunwaldt and co-workers engineered a continuous microfluidic setup that reduced $HAuCl_4$ with sodium borohydride ($NaBH_4$) in the presence of PVP to synthesize ultrasmall Au NPs with catalytic applications in mind.[69] Specifically, the setup used pressurized vessels that allowed pulsation-free flow of reactants in a microfluidic chip with integrated mixers. Furthermore, this chip enabled recordings of X-ray absorption spectra in situ, showing oxidized Au was observed after 6 ms and only metallic Au was observed after 10 ms. Further ex situ characterization

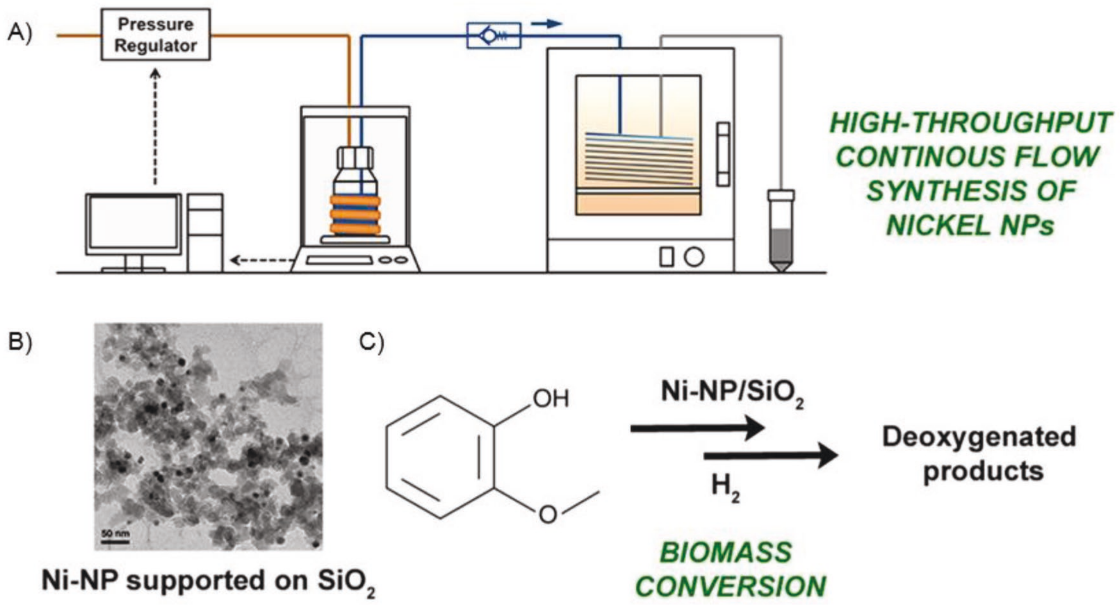

Figure 9. Top: Scheme of the reactor used for synthesizing Ni NPs in a high-throughput continuous method. Bottom: TEM image of Ni NPs supported on SiO$_2$ and a reaction scheme for the hydrodeoxygenation of guaiacol. Adapted with permission.[67] Copyright 2017, American Chemical Society.

techniques showed the final Au NPs had an average diameter of 1.0 nm, with narrow size distributions. After depositing the Au NPs on TiO$_2$, these supported catalysts showed good catalytic performance for CO oxidation. In related studies, Jamal and co-workers developed a microfluidic method to load 1–2 nm Au NPs in silica capillaries for fine organic transformations, showing the ability to integrate synthesis of the catalytically active phase with deposition on supports through flow strategies.[70] This methodology should be applicable to a diversity of support materials and a variety of chemical transformations, including CO oxidation.[71]

6.2. Bimetallic Systems

Batch syntheses of bimetallic NPs with catalytic capabilities have also been demonstrated. Ag–Au NPs synthesized in batch have shown excellent capabilities in catalyzing CO oxidation as there is a strong synergism in the coadsorption of CO and O$_2$ on the Au–Ag nanoparticle surface.[72] Recently, Mayer and co-workers designed microreactors composed of static micromixers (made via microlithographic Si/glass chip technology) and PTFE tubes for flow-through reactions producing Ag–Au NPs with different ratios of Ag and Au.[73] The NP syntheses were based on reduction of tetrachloroauric acid and silver nitrate with NaBH$_4$. The size of the NPs and the product monodispersity were dependent on the metal-to-metal ratio and the order that reagent species were added inline. The catalytic performances of the Ag–Au NPs were evaluated through bleaching of organic dyes with potassium peroxodisulfate. The NPs with the highest Ag-to-Au ratio exhibited the greatest enhancement in bleaching rate, whereas no catalytic activity was demonstrated with NPs composed only of Au. This study shows microreactor compositional control of NPs and how this control can lead to product performance.

Additionally, Pt–Ni NPs made in batch syntheses have good catalytic behavior, especially toward ORR.[74] In 2016, Xia and co-workers demonstrated the synthesis of Pt–Ni octahedra in a continuous-flow droplet reactor, and the Pt–Ni NPs exhibited remarkable activity toward ORR.[75] This study pumped all reagent material into the reaction tubing using only one syringe and one syringe pump. The reagent syringe contained an oleylamine solution with Pt(acac)$_2$, Ni(acac)$_2$, and W(CO)$_6$. The separation between reaction droplets was created by CO gas as W(CO)$_6$ decomposed during the reaction. Thus, this microreactor did not use a typical immiscible carrier fluid. The reaction droplets were fed into a heated zone held between 170 and 230 °C. After the reaction droplets were heated, they exited the reaction tubing and were collected in a vial. The microreactor setup and Pt–Ni products can be seen in **Figure 10**.[75] The size and composition of the Pt–Ni octahedra were controlled through solvent manipulations and metal precursor concentrations in the initial precursor solution, not through process parameters inherent to the microreactor. To evaluate catalytic performance, Pt$_{2.4}$Ni octahedra with a 9 nm edge length were chosen and showed an ORR mass activity of 2.67 A $\text{mg}_{\text{Pt}}^{-1}$ at 0.9 V. This activity is an 11-fold improvement over a state-of-the-art commercial Pt/C catalyst (0.24 A $\text{mg}_{\text{Pt}}^{-1}$). Similar products have been made in batch reactors, but their yield is typically on the scale of 5–25 mg Pt per batch, which is not enough for industrial commercialization. Using the continuous-flow droplet microreactor approach, 20 mg h^{-1} of 9 nm Pt–Ni product was achieved. This yield was further advanced when the diameter of the PTFE reaction tubing was increased to 3.0 mm, creating larger reaction droplets to generate 160 mg h^{-1} of Pt–Ni product. This study not only shows the synthetic capabilities and versatility of microreactors for NP synthesis, it also demonstrates the ability to make effective nanocatalysts in a product volume that cannot be achieved by batch reactors.

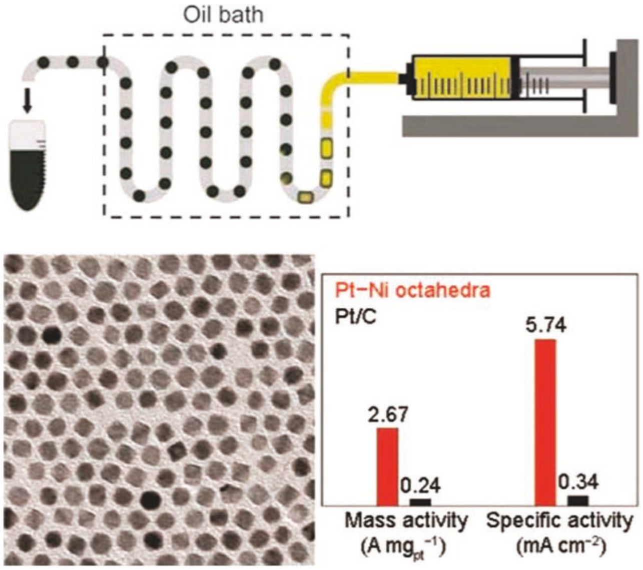

Figure 10. A scheme of the continuous-droplet reactor used to synthesize Pt–Ni octahedra, a TEM image of the Pt–Ni octahedral product, and a graphical representation of the Pt–Ni octahedra activity toward ORR compared to the commercial Pt/C activity. Adapted with permission.[75] Copyright 2016, American Chemical Society.

Lastly, this microreactor methodology can be extended to core@shell oxide structures for enhanced photocatalytic activity. A photocatalyst is a catalyst that requires or engages light, with metal oxides being common materials for this process.[74] In 2017, Chen and co-workers synthesized core@shell Ag@Cu$_2$O NPs in a multistep microfluidic method.[76] In the first stage of their microreactor, Cu(OH)$_4^{2-}$ was formed by reacting CuSO$_4$ with NaOH. Next, core@shell Ag@Cu$_2$O NPs were formed by reducing the Cu(OH)$_4^{2-}$ with L-aa in the presence of triangular Ag nanoprisms. In-depth characterization of the core@shell Ag@Cu$_2$O product revealed the Cu$_2$O shell was polycrystalline in nature with epitaxially domains growing on the Ag nanoprisms. The core@shell Ag@Cu$_2$O NPs were compared to pristine Cu$_2$O NPs for the visible light–driven degradation of methyl orange. The core@shell Ag@Cu$_2$O NPs showed superior activity compared to the Cu$_2$O particles. Enhanced performance for the core@shell particles was attributed to the larger surface area and improved charge separation within the material compared to the reference. Furthermore, no obvious deactivation from the core@shell Ag@Cu$_2$O NPs was observed during repeated testing. This study demonstrates that microreactor technology can be extended to synthesizing a variety of catalysts, not only pure metallic NPs.

6.3. Hierarchical Systems

Hierarchical systems are drawing attention in catalysis for their multicomponent and layered systems which can give rise to enhanced performance.[77] These hierarchical systems typically require elaborate synthetic strategies. In 2018, Li et al. used microreactor technology to assemble hierarchical multicomponent particles.[78] These particles were composed of metal NPs (Au, Ag, and Rh) uniformly distributed on sub-micrometer-sized polymer particles. Furthermore, these metal NP/ polymer networks were combined with polyacrylamide (PAA) hydrogel particles to form hierarchical assemblies. The metal NPs, polymer particles, and PAA hydrogel were all prepared separately in microreactors, with the assemblies built by combining the materials in a batch system. After assembly, this material was evaluated as a catalyst for the reductive bleaching of an azo dye by NaBH$_4$. The results showed this hierarchical network was an effective catalyst, with an enhanced rate of bleaching reported. This study shows the versatile promise of synthetic design for NPs by combining different materials into a multicomponent hierarchical network.

7. Closing Vision

As Section 2 of this progress report outlines, control over NP composition, size, shape, and architecture can give rise to enhanced catalytic performance. The correlation between NP structure and performance has largely been established from the study of NPs synthesized by small batch methods. However, synthesizing such designer NPs in batch reactions limits scale-up. Sections 5 and 6 highlight droplet microreactor routes to metal NPs, with some examples reporting both large production rates and fine structural and compositional control. Given that the ability of droplet microreactors to produce high-quality metal NPs for applications in catalysis has been demonstrated, now is the time to take advantage of the unique features of droplet microreactors and 1) achieve designer nanocatalysts not possible through batch pathways and 2) integrate inline characterization and catalysis.

7.1. New Nanostructures

In considering the synthetic opportunities that arise from droplet microreactors, the ability to rapidly screen synthetic conditions is an attribute. As mentioned throughout the progress report, synthetic versatility in microreactor reactions for product diversity is an advantage. In 2016, Sebastián and Jensen reported the synthesis of a variety of known and new metal NPs through small manipulations to microreactor reactions.[37e] Specifically, monometallic and bimetallic spherical NPs, nanodendrites, nanocubes, core@shell NPs, Janus nanostructures, dumbbells, nanorods, and nanosheets were all synthesized through small changes to flow patterns and synthetic conditions. Moreover, this synthetic method gave rise to nanostructures hitherto not reported such as Pt–Ru, Pt–Ni, and Pt–Co nanodendrites, Pt–Pd heterostructures, Ag–Pd core@shell NPs, Au–Pd nanodumbbells, and Au–Pd nanosheets. The silicon–Pyrex microfluidic reactor used for all reactions allowed reagents to be mixed inline before entering a hot area capable of initiating the NP growth. This setup was capable of simple modifications (temperature, pressure, reactants, residence time, and flow conditions) giving rise to a library of metallic nanostructures with different compositions, sizes, shapes, and architectures. The metal domains, exposed facets, and the ε_d of the final NPs will tailor different catalytic performances. By combining this synthetic versatility with the scale-up advantage of microreactors, new catalysts can be evaluated with possible production on the industrial scale.

Moreover, the droplets can be viewed as spatially and temporally confined reaction vessels, potentially providing unique chemical environments. For example, the spatial and temporal confinement of aerosol droplets have enabled molten salt syntheses to be spatially and temporally confined, providing a pathway to shape-controlled nanoparticles through control of supersaturation conditions; traditionally molten salt syntheses produce micrometer-sized crystals.[37c] In the case of droplet microreactors, a diversity of different chemistries can similarly be confined, which may give rise to unique synthetic outcomes.

Also, the flow nature of the droplet microreactors allows different reaction events to occur sequentially inline. Section 5.8 introduced the idea of multistep processes, in one example through viable temperatures inline and in a second example through the electrocoalescence of droplets. A largely unexplored concept is the introduction of other energy sources (e.g., electromagnetic radiation or ultrasound) at specific points inline. In the case of metal NP synthesis, light in the visible to near-IR regions is capable of plasmon-driven synthesis, which has been particularly useful in accessing kinetic nanostructures (i.e., those expressing high energy facets or of anisotropic shape) of Au, Ag, and other metals capable of sustaining a plasmon in that region.[79] Furthermore, a large variety of metal NPs have been synthesized through microwave heating, where the formation of NPs is reportedly faster and with narrower size distributions compared to conventional heating.[80] Thus, the ability to deliver electromagnetic radiation of specific energies and intensities at different points inline could provide access to completely new NPs, including kinetic nanostructures and metastable phases.

Finally, the interface between the droplet and carrier phase has been hardly explored to access new types of metal nanostructures. However, this interface is a unique feature of droplet microreactors at which chemistry can occur. For example, silica microcapsules (hollow spheres) have been produced due to growth reactions occurring at the oil/water interface.[81] The silica microcapsules were formed by stabilizing the interface during growth. Potentially, this methodology can be extended to metal nanoparticle growth as many growth directing agents can interact at the water/oil interface, allowing the curvature of the interface to possibly facilitate shape control. NP self-assemblies can also occur at the interface, giving the possibility of achieving a thin film for catalysis.[82] Additionally, a variety of different flow methods have been used to produce multicompartment microdroplets. These microstructures typically form from the immiscibility of different polymer domains but also provide a mechanism to confine incompatible reagents spatially so that mixing and reaction can be initiated downstream. These multicompartment microdroplets may also allow different reactions to occur within each compartment and create unique heterostructures with defined interfaces. This possibility is particularly attractive to the design of catalysts where grain boundaries have been identified as active sites in many cases.

7.2. Inline Catalysis

Just as flow chemistry has been developing for the synthesis of metal NPs, continuous flow microreactors have been developing for catalyst testing and deployment. These microreactors similarly offer improved heat and mass transfer, which can improve the selectivity of many catalysts. Additionally, the use of alternative means of energy transfer (e.g., ultrasound or microwave radiation) within microreactors has been shown to increase reaction rates. With these, and other, advantages in mind, the ability to integrate metal NP synthesis, characterization, and catalysis all in one stream becomes attractive.

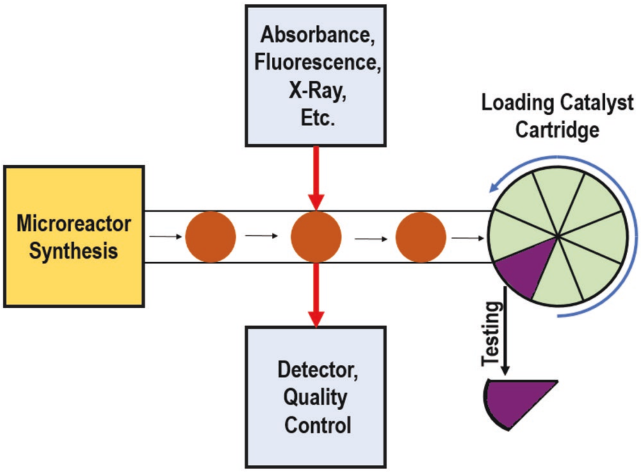
Absorbance, Fluorescence, X-Ray, Etc.
Loading Catalyst Cartridge
Microreactor Synthesis
Testing
Detector, Quality Control

Figure 11. A scheme showing the process of synthesizing NPs in a microreactor, online analyses for quality control, and cartridge loading for catalytic applications.

For example, metal NP synthesis can proceed using the methods described in Sections 5 and 6, with different reaction conditions being screened. The products from these syntheses can then be characterized by a variety of different methods. Typically, absorption and fluorescence measurements are used to extract size distributions and surface uniformity.[83] Online characterization is starting to expand to Raman, X-ray, and nuclear magnetic resonance spectroscopy for reaction monitoring and catalyst characterization.[55] The various products can then be delivered further downstream to cartridges that immobilize the NPs on a catalyst support that is then detached from the synthesis portion of the microreactor. Now, nanocatalyst cleaning and activation can proceed using the methods developed for heterogeneous catalysts in continuous flow microreactors, followed by testing. The overall concept is depicted in **Figure 11**. Altogether, this type of microreactor provides a combinatorial and automated approach to metal NP synthesis, characterization, and catalyst evaluation. For this vision to be realized, advanced understanding of NP synthesis and catalyst evaluation in flow reactors is required, along with automated sample handling, analytical testing and data analysis.

Acknowledgements

The authors acknowledge financial support from U.S. DOE BES Award DE-SC0018961 and NSF CHE-1602476 and CHE-1904499.

Conflict of Interest

The authors declare no conflict of interest.

Keywords

catalysis, microreactors, nanocrystals, nanoparticles, scale-up

Received: June 25, 2019
Revised: August 5, 2019
Published online: September 5, 2019

[1] a) E. C. Dreaden, M. A. Mackey, X. Huang, B. Kang, M. A. El-Sayed, *Chem. Soc. Rev.* **2011**, *40*, 3391; b) D. Cassano, S. Pocoví-Martínez, V. Voliani, *Bioconjugate Chem.* **2018**, *29*, 4; c) W. P. Hall, S. N. Ngatia, R. P. Van Duyne, *J. Phys. Chem. C* **2011**, *115*, 1410; d) K. C. Ng, F.-C. Lin, P.-W. Yang, Y.-C. Chuang, C.-K. Chang, A.-H. Yeh, C.-S. Kuo, C.-R. Kao, C.-C. Liu, U. S. Jeng, J.-S. Huang, C.-H. Kuo, *Chem. Mater.* **2018**, *30*, 204; e) K. A. Willets, R. P. V. Duyne, *Annu. Rev. Phys. Chem.* **2007**, *58*, 267; f) B. Song, H. Wang, Y. Zhong, B. Chu, Y. Su, Y. He, *Nanoscale* **2018**, *10*, 1617.

[2] Y. Li, G. A. Somorjai, *Nano Lett.* **2010**, *10*, 2289.

[3] a) B. C. H. Steele, A. Heinzel, *Nature* **2001**, *414*, 345; b) M. Winter, R. J. Brodd, *Chem. Rev.* **2004**, *104*, 4245.

[4] J. T. L. Gamler, H. M. Ashberry, S. E. Skrabalak, K. M. Koczkur, *Adv. Mater.* **2018**, *30*, 1801563.

[5] L. Delannoy, N. El Hassan, A. Musi, N. N. Le To, J.-M. Krafft, C. Louis, *J. Phys. Chem. B* **2006**, *110*, 22471.

[6] a) M. Kim, Y. Kim, J. W. Hong, S. Ahn, W. Y. Kim, S. W. Han, *Chem. Commun.* **2014**, *50*, 9454; b) K. Zhou, Y. Li, *Angew. Chem., Int. Ed.* **2012**, *51*, 602; c) C.-W. Yang, K. Chanda, P.-H. Lin, Y.-N. Wang, C.-W. Liao, M. H. Huang, *J. Am. Chem. Soc.* **2011**, *133*, 19993; d) C.-Y. Chiu, P.-J. Chung, K.-U. Lao, C.-W. Liao, M. H. Huang, *J. Phys. Chem. C* **2012**, *116*, 23757; e) Y. Wu, S. Cai, D. Wang, W. He, Y. Li, *J. Am. Chem. Soc.* **2012**, *134*, 8975; f) M. Crespo-Quesada, A. Yarulin, M. Jin, Y. Xia, L. Kiwi-Minsker, *J. Am. Chem. Soc.* **2011**, *133*, 12787; g) Y.-T. Chu, K. Chanda, P.-H. Lin, M. H. Huang, *Langmuir* **2012**, *28*, 11258.

[7] Y. Xia, Y. Xiong, B. Lim, S. E. Skrabalak, *Angew. Chem., Int. Ed.* **2009**, *48*, 60.

[8] a) K. M. Koczkur, S. Mourdikoudis, L. Polavarapu, S. E. Skrabalak, *Dalton Trans.* **2015**, *44*, 17883; b) S. Mourdikoudis, L. M. Liz-Marzán, *Chem. Mater.* **2013**, *25*, 1465; c) Y. Yan, K.-b. Chen, H.-r. Li, W. Hong, X.-b. Hu, Z. Xu, *Trans. Nonferrous Met. Soc. China* **2014**, *24*, 3732; d) N. Naresh, F. G. S. Wasim, B. P. Ladewig, M. Neergat, *J. Mater. Chem. A* **2013**, *1*, 8553; e) H. Huang, Y. Wang, A. Ruditskiy, H.-C. Peng, X. Zhao, L. Zhang, J. Liu, Z. Ye, Y. Xia, *ACS Nano* **2014**, *8*, 7041.

[9] Y. Wang, H.-C. Peng, J. Liu, C. Z. Huang, Y. Xia, *Nano Lett.* **2015**, *15*, 1445.

[10] G. Niu, A. Ruditskiy, M. Vara, Y. Xia, *Chem. Soc. Rev.* **2015**, *44*, 5806.

[11] A. R. Zeradjanin, J.-P. Grote, G. Polymeros, K. J. J. Mayrhofer, *Electroanalysis* **2016**, *28*, 2256.

[12] a) B. Hammer, J. K. Norskov, *Nature* **1995**, *376*, 238; b) B. Hammer, Y. Morikawa, J. K. Nørskov, *Phys. Rev. Lett.* **1996**, *76*, 2141.

[13] E. Toyoda, R. Jinnouchi, T. Hatanaka, Y. Morimoto, K. Mitsuhara, A. Visikovskiy, Y. Kido, *J. Phys. Chem. C* **2011**, *115*, 21236.

[14] a) T. Bligaard, J. K. Nørskov, *Electrochim. Acta* **2007**, *52*, 5512; b) K. Jiang, H.-X. Zhang, S. Zou, W.-B. Cai, *Phys. Chem. Chem. Phys.* **2014**, *16*, 20360.

[15] V. R. Stamenkovic, B. S. Mun, M. Arenz, K. J. J. Mayrhofer, C. A. Lucas, G. Wang, P. N. Ross, N. M. Markovic, *Nat. Mater.* **2007**, *6*, 241.

[16] a) S. Furukawa, T. Komatsu, *ACS Catal.* **2017**, *7*, 735; b) P. Liu, J. K. Nørskov, *Phys. Chem. Chem. Phys.* **2001**, *3*, 3814.

[17] a) R. V. Maligal-Ganesh, C. Xiao, T. W. Goh, L.-L. Wang, J. Gustafson, Y. Pei, Z. Qi, D. D. Johnson, S. Zhang, F. Tao, W. Huang, *ACS Catal.* **2016**, *6*, 1754; b) R. E. Cable, R. E. Schaak, *Chem. Mater.* **2005**, *17*, 6835; c) N. H. Chou, R. E. Schaak, *J. Am. Chem. Soc.* **2007**, *129*, 7339.

[18] K. D. Gilroy, A. Ruditskiy, H.-C. Peng, D. Qin, Y. Xia, *Chem. Rev.* **2016**, *116*, 10414.

[19] a) Z. Chen, X. Zhang, G. Lu, *J. Phys. Chem. C* **2017**, *121*, 1964; b) X. X. Wang, S. Hwang, Y.-T. Pan, K. Chen, Y. He, S. Karakalos, H. Zhang, J. S. Spendelow, D. Su, G. Wu, *Nano Lett.* **2018**, *18*, 4163; c) J. T. L. Gamler, A. Leonardi, H. M. Ashberry, N. N. Daanen, Y. Losovyj, R. R. Unocic, M. Engel, S. E. Skrabalak, *ACS Nano* **2019**, *13*, 4008.

[20] C. Wang, D. P. Chen, X. Sang, R. R. Unocic, S. E. Skrabalak, *ACS Nano* **2016**, *10*, 6345.

[21] G. A. Somorjai, J. Y. Park, *Angew. Chem., Int. Ed.* **2008**, *47*, 9212.

[22] K. An, G. A. Somorjai, *ChemCatChem* **2012**, *4*, 1512.

[23] M. Shao, A. Peles, K. Shoemaker, *Nano Lett.* **2011**, *11*, 3714.

[24] a) C. J. Kliewer, C. Aliaga, M. Bieri, W. Huang, C.-K. Tsung, J. B. Wood, K. Komvopoulos, G. A. Somorjai, *J. Am. Chem. Soc.* **2010**, *132*, 13088; b) C.-K. Tsung, J. N. Kuhn, W. Huang, C. Aliaga, L.-I. Hung, G. A. Somorjai, P. Yang, *J. Am. Chem. Soc.* **2009**, *131*, 5816; c) G. L. Bezemer, J. H. Bitter, H. P. C. E. Kuipers, H. Oosterbeek, J. E. Holewijn, X. Xu, F. Kapteijn, A. J. van Dillen, K. P. de Jong, *J. Am. Chem. Soc.* **2006**, *128*, 3956.

[25] J. N. Kuhn, W. Huang, C.-K. Tsung, Y. Zhang, G. A. Somorjai, *J. Am. Chem. Soc.* **2008**, *130*, 14026.

[26] a) C. Burda, X. Chen, R. Narayanan, M. A. El-Sayed, *Chem. Rev.* **2005**, *105*, 1025; b) G. A. Somorjai, D. W. Blakely, *Nature* **1975**, *258*, 580; c) N. M. Markovic, H. A. Gasteiger, P. N. Ross, *J. Phys. Chem.* **1995**, *99*, 3411.

[27] a) E. M. Karp, T. L. Silbaugh, C. T. Campbell, *J. Am. Chem. Soc.* **2013**, *135*, 5208; b) J. L. Brand, M. V. Arena, A. A. Deckert, S. M. George, *J. Chem. Phys.* **1990**, *92*, 5136; c) M. D. Alvey, J. T. Yates, K. J. Uram, *J. Chem. Phys.* **1987**, *87*, 7221.

[28] W. Zhou, J. Wu, H. Yang, *Nano Lett.* **2013**, *13*, 2870.

[29] Y. Xia, X. Xia, H.-C. Peng, *J. Am. Chem. Soc.* **2015**, *137*, 7947.

[30] A. J. Biacchi, R. E. Schaak, *ACS Nano* **2011**, *5*, 8089.

[31] J. Zeng, Q. Zhang, J. Chen, Y. Xia, *Nano Lett.* **2010**, *10*, 30.

[32] B. T. Sneed, A. P. Young, C. K. Tsung, *Nanoscale* **2015**, *7*, 12248.

[33] F.-R. Fan, D.-Y. Liu, Y.-F. Wu, S. Duan, Z.-X. Xie, Z.-Y. Jiang, Z.-Q. Tian, *J. Am. Chem. Soc.* **2008**, *130*, 6949.

[34] J. Hora, C. Hall, D. Evans, E. Charrault, *Adv. Eng. Mater.* **2018**, *20*, 1700868.

[35] J. Park, J. Joo, S. G. Kwon, Y. Jang, T. Hyeon, *Angew. Chem., Int. Ed.* **2007**, *46*, 4630.

[36] L. Zhang, Y. Xia, *Adv. Mater.* **2014**, *26*, 2600.

[37] a) G. M. Whitesides, *Nature* **2006**, *442*, 368; b) C.-X. Zhao, L. He, S. Z. Qiao, A. P. J. Middelberg, *Chem. Eng. Sci.* **2011**, *66*, 1463; c) S. E. Skrabalak, R. L. Brutchey, *Chem. Mater.* **2016**, *28*, 1003; d) L.-J. Pan, J.-W. Tu, H.-T. Ma, Y.-J. Yang, Z.-Q. Tian, D.-W. Pang, Z.-L. Zhang, *Lab Chip* **2018**, *18*, 41; e) V. Sebastián, K. F. Jensen, *Nanoscale* **2016**, *8*, 15288; f) E. J. Roberts, L. R. Karadaghi, L. Wang, N. Malmstadt, R. L. Brutchey, *ACS Appl. Mater. Interfaces* **2019**, *11*, 27479.

[38] a) A. Knauer, A. Csaki, F. Möller, C. Hühn, W. Fritzsche, J. Köhler, *J. Phys. Chem. C* **2012**, *116*, 9251; b) S. Tao, M. Yang, H. Chen, S. Zhao, G. Chen, *Ind. Eng. Chem. Res.* **2018**, *57*, 3263.

[39] J. S. Santana, K. M. Koczkur, S. E. Skrabalak, *Langmuir* **2017**, *33*, 6054.

[40] S.-Y. Teh, R. Lin, L.-H. Hung, A. P. Lee, *Lab Chip* **2008**, *8*, 198.

[41] Y. H. Kim, L. Zhang, T. Yu, M. Jin, D. Qin, Y. Xia, *Small* **2013**, *9*, 3462.

[42] a) S. Duraiswamy, S. A. Khan, *Nano Lett.* **2010**, *10*, 3757; b) L. L. Lazarus, C. T. Riche, B. C. Marin, M. Gupta, N. Malmstadt, R. L. Brutchey, *ACS Appl. Mater. Interfaces* **2012**, *4*, 3077.

[43] a) S. M. Madren, M. D. Hoffman, P. J. B. Brown, D. T. Kysela, Y. V. Brun, S. C. Jacobson, *Anal. Chem.* **2012**, *84*, 8571;

b) J. H. Bannock, S. H. Krishnadasan, M. Heeney, J. C. de Mello, *Mater. Horiz.* **2014**, *1*, 373; c) A.-C. Bédard, A. Adamo, K. C. Aroh, M. G. Russell, A. A. Bedermann, J. Torosian, B. Yue, K. F. Jensen, T. F. Jamison, *Science* **2018**, *361*, 1220; d) Z. V. Feng, K. R. Edelman, B. P. Swanson, *J. Chem. Educ.* **2015**, *92*, 723; e) A. Toyota, H. Nakamura, H. Ozono, K. Yamashita, M. Uehara, H. Maeda, *J. Phys. Chem. C* **2010**, *114*, 7527.
[44] L. Zhang, Y. Wang, L. Tong, Y. Xia, *Nano Lett.* **2014**, *14*, 4189.
[45] D. Liu, H. Zhang, S. Cito, J. Fan, E. Mäkilä, J. Salonen, J. Hirvonen, T. M. Sikanen, D. A. Weitz, H. A. Santos, *Nano Lett.* **2017**, *17*, 606.
[46] J.-M. Lim, A. Swami, L. M. Gilson, S. Chopra, S. Choi, J. Wu, R. Langer, R. Karnik, O. C. Farokhzad, *ACS Nano* **2014**, *8*, 6056.
[47] a) H. Song, J. D. Tice, R. F. Ismagilov, *Angew. Chem., Int. Ed.* **2003**, *42*, 768; b) B. K. H. Yen, A. Günther, M. A. Schmidt, K. F. Jensen, M. G. Bawendi, *Angew. Chem.* **2005**, *117*, 5583; c) H. Song, M. R. Bringer, J. D. Tice, C. J. Gerdts, R. F. Ismagilov, *Appl. Phys. Lett.* **2003**, *83*, 4664.
[48] L. Frenz, A. El Harrak, M. Pauly, S. Bégin-Colin, A. D. Griffiths, J.-C. Baret, *Angew. Chem., Int. Ed.* **2008**, *47*, 6817.
[49] a) C. Priest, S. Herminghaus, R. Seemann, *Appl. Phys. Lett.* **2006**, *89*, 134101; b) K. Ahn, J. Agresti, H. Chong, M. Marquez, D. A. Weitz, *Appl. Phys. Lett.* **2006**, *88*, 264105.
[50] T. Gu, C. Zheng, F. He, Y. Zhang, S. A. Khan, T. A. Hatton, *Lab Chip* **2018**, *18*, 1330.
[51] a) A. Knauer, A. Thete, S. Li, H. Romanus, A. Csáki, W. Fritzsche, J. M. Köhler, *Chem. Eng. J.* **2011**, *166*, 1164; b) L. Zhang, G. Niu, N. Lu, J. Wang, L. Tong, L. Wang, M. J. Kim, Y. Xia, *Nano Lett.* **2014**, *14*, 6626.
[52] A. M. Nightingale, J. H. Bannock, S. H. Krishnadasan, F. T. F. O'Mahony, S. A. Haque, J. Sloan, C. Drury, R. McIntyre, J. C. deMello, *J. Mater. Chem. A* **2013**, *1*, 4067.
[53] D. Conchouso, D. Castro, S. A. Khan, I. G. Foulds, *Lab Chip* **2014**, *14*, 3011.
[54] C. T. Riche, E. J. Roberts, M. Gupta, R. L. Brutchey, N. Malmstadt, *Nat. Commun.* **2016**, *7*, 10780.
[55] J. Yue, F. H. Falke, J. C. Schouten, T. A. Nijhuis, *Lab Chip* **2013**, *13*, 4855.
[56] P. Kunal, E. J. Roberts, C. T. Riche, K. Jarvis, N. Malmstadt, R. L. Brutchey, S. M. Humphrey, *Chem. Mater.* **2017**, *29*, 4341.
[57] S. Garcia, G. W. Piburn, S. M. Humphrey, in *Microwave Engineering of Materials and Nanomaterials—From Mesoscale to Nanoscale* (Ed: E. Guenin), Pan Stanford Publishing Pte. Ltd., Singapore **2016**.
[58] G. H. Albuquerque, K. Squire, A. X. Wang, G. S. Herman, *Cryst. Growth Des.* **2018**, *18*, 119.
[59] J. S. Santana, J. T. L. Gamler, S. E. Skrabalak, *Part. Part. Syst. Charact.* **2019**, 1900142.
[60] a) B. Lim, M. Jiang, P. H. C. Camargo, E. C. Cho, J. Tao, X. Lu, Y. Zhu, Y. Xia, *Science* **2009**, *324*, 1302; b) B. Lim, M. Jiang, T. Yu, P. H. C. Camargo, Y. Xia, *Nano Res.* **2010**, *3*, 69; c) L. Wang, Y. Nemoto, Y. Yamauchi, *J. Am. Chem. Soc.* **2011**, *133*, 9674; d) S. Guo, S. Dong, E. Wang, *ACS Nano* **2010**, *4*, 547; e) S. Xie, S.-I. Choi, N. Lu, L. T. Roling, J. A. Herron, L. Zhang, J. Park, J. Wang, M. J. Kim, Z. Xie, M. Mavrikakis, Y. Xia, *Nano Lett.* **2014**, *14*, 3570.
[61] a) H. Wang, Z. Sun, Y. Yang, D. Su, *Nanoscale* **2013**, *5*, 139; b) W. Zhou, J. Y. Lee, *Electrochem. Commun.* **2007**, *9*, 1725.
[62] J. S. Santana, K. M. Koczkur, S. E. Skrabalak, *React. Chem. Eng.* **2018**, *3*, 437.
[63] M. Fricke, K. Sundmacher, *Langmuir* **2012**, *28*, 6803.
[64] K. Kumar, A. D. Nikolov, D. T. Wasan, *J. Colloid Interface Sci.* **2002**, *256*, 194.
[65] A. A. Kulkarni, V. Sebastian Cabeza, *Langmuir* **2017**, *33*, 14315.
[66] Ö. Metin, V. Mazumder, S. Özkar, S. Sun, *J. Am. Chem. Soc.* **2010**, *132*, 1468.
[67] E. J. Roberts, S. E. Habas, L. Wang, D. A. Ruddy, E. A. White, F. G. Baddour, M. B. Griffin, J. A. Schaidle, N. Malmstadt, R. L. Brutchey, *ACS Sustainable Chem. Eng.* **2017**, *5*, 632.
[68] G. C. Bond, P. A. Sermon, *Gold Bull.* **1973**, *6*, 102.
[69] G. Tofighi, H. Lichtenberg, J. Pesek, T. L. Sheppard, W. Wang, L. Schöttner, G. Rinke, R. Dittmeyer, J.-D. Grunwaldt, *React. Chem. Eng.* **2017**, *2*, 876.
[70] F. Jamal, G. Jean-Sébastien, P. Maël, P. Edmond, R. Christian, *Microsyst. Technol.* **2012**, *18*, 151.
[71] M. Haruta, N. Yamada, T. Kobayashi, S. Iijima, *J. Catal.* **1989**, *115*, 301.
[72] A.-Q. Wang, C.-M. Chang, C.-Y. Mou, *J. Phys. Chem. B* **2005**, *109*, 18860.
[73] J. M. Köhler, L. Abahmane, J. Wagner, J. Albert, G. Mayer, *Chem. Eng. Sci.* **2008**, *63*, 5048.
[74] S. Kühl, M. Gocyla, H. Heyen, S. Selve, M. Heggen, R. E. Dunin-Borkowski, P. Strasser, *J. Mater. Chem. A* **2019**, *7*, 1149.
[75] G. Niu, M. Zhou, X. Yang, J. Park, N. Lu, J. Wang, M. J. Kim, L. Wang, Y. Xia, *Nano Lett.* **2016**, *16*, 3850.
[76] S. Tao, M. Yang, H. Chen, M. Ren, G. Chen, *J. Colloid Interface Sci.* **2017**, *486*, 16.
[77] Z. Ren, Y. Guo, C.-H. Liu, P.-X. Gao, *Front. Chem.* **2013**, *1*, 18.
[78] X. Li, N. R. Visaveliya, L. Hafermann, A. Knauer, S. Schneider, J. M. Köhler, *ACS Appl. Nano Mater.* **2018**, *1*, 6398.
[79] R. Kamarudheen, G. W. Castellanos, L. P. J. Kamp, H. J. H. Clercx, A. Baldi, *ACS Nano* **2018**, *12*, 8447.
[80] C. B. Collins, R. S. McCoy, B. J. Ackerson, G. J. Collins, C. J. Ackerson, *Nanoscale* **2014**, *6*, 8459.
[81] M. Fujiwara, K. Shiokawa, Y. Tanaka, Y. Nakahara, *Chem. Mater.* **2004**, *16*, 5420.
[82] L. L. Dai, R. Sharma, C.-y. Wu, *Langmuir* **2005**, *21*, 2641.
[83] T. W. Phillips, I. G. Lignos, R. M. Maceiczyk, A. J. deMello, J. C. deMello, *Lab Chip* **2014**, *14*, 3172.